HO_x Observation and Model Comparison during INTEX-A 2004

Xinrong Ren*,[1] Jennifer R. Olson,[2] James H. Crawford,[2] William H. Brune,[1] Jingqiu Mao,[1] Robert B. Long,[1] Gao Chen,[2] Melody A. Avery,[2] Glen W. Sachse,[2] John D. Barrick,[2] Glenn S. Diskin,[2] L. Greg Huey,[3] Alan Fried,[4] Ronald C. Cohen,[5] Brian Heikes,[6] Paul Wennberg,[7] Hanwant B. Singh,[8] Donald R. Blake,[9] Richard E. Shetter[10]

[1]*Department of Meteorology, Pennsylvania State University, University Park, PA, USA*

[2]*Atmospheric Science Division, NASA Langley Research Center, Hampton, VA, USA*

[3]*School of Earth and Atmospheric Sciences, Georgia Institute of Technology, Atlanta, GA, USA*

[4]*Atmospheric Chemistry Division, National Center for Atmospheric Research, Boulder, CO, USA*

[5]*Department of Chemistry and Department of Earth and Planetary Science, University of California Berkeley, Berkeley, CA, USA*

[6]*Graduate School of Oceanography, University of Rhode Island, Narragansett, RI, USA*

[7]*Division of Engineering and Applied Sciences, California Institute of Technology, Pasadena, CA, USA.*

[8]*NASA Ames Research Center, Moffett Field, CA, USA.*

[9]*Department of Earth System Science, University of California, Irvine, CA, USA.*

[10]*National Suborbital Education & Research Center, University of North Dakota, Grand Forks, ND, USA*

*Correspondence to: X. Ren (xur1@psu.edu)

Resubmitted to Journal of Geophysical Research
INTEX-A/ICARTT Special Issue

30 September, 2006

Abstract. OH and HO_2 were measured with the Airborne Tropospheric Hydrogen Oxides Sensor (ATHOS) as part of a large measurement suite from the NASA DC-8 aircraft during the Intercontinental Chemical Transport Experiment – A (INTEX-A). This mission, which was conducted mainly over North America and the western Atlantic Ocean in summer 2004, was an excellent test of atmospheric oxidation chemistry. Throughout the troposphere, observed OH was generally 0.60 of the modeled OH; below 8 km, observed HO_2 was generally 0.78 of modeled HO_2. If the over-prediction of tropospheric OH is not due to an instrument calibration error, then it implies less global tropospheric oxidation capacity and longer lifetimes for gases like methane and methyl chloroform than currently thought. This discrepancy falls well outside uncertainties in both the OH measurement and rate coefficients for known reactions and points to a large unknown OH loss. If the modeled OH is forced to agree with observed values by introducing of an undefined OH loss that removes HO_x (HO_x=OH+HO_2), the observed and modeled HO_2 and HO_2/OH ratios are largely reconciled within the measurement uncertainty. HO_2 behavior above 8 km was markedly different. The observed-to-modeled HO_2 ratio increased from ~1 at 8 km to more ~2.5 at 11 km with the observed-to-modeled ratio correlating with NO. The observed-to-modeled HO_2 and NO were both considerably greater than observations from previous campaigns. In addition, the observed-to-modeled HO_2/OH, which is sensitive to cycling reactions between OH and HO_2, increased from ~1.2 at 8 km to almost 4 above 11 km. In contrast to the lower atmosphere, these discrepancies above 8 km suggest a large unknown HO_x source and additional reactants that cycle HO_x from OH to HO_2. In the continental planetary boundary layer, the OH observed-to-modeled ratio increased from 0.6 when isoprene was less than 0.1 ppbv to over 3 when isoprene was greater than 2 ppbv, suggesting that forests throughout the United States are emitting unknown HO_x sources. Progress in resolving these

discrepancies requires further examination of possible unknown OH sinks and HO_x sources and a focused research activity devoted to ascertaining the accuracy of the OH and HO_2 measurements.

Index terms:

0365 Atmospheric Composition and Structure: Troposphere—composition and chemistry;

0368 Atmospheric Composition and Structure: constituent transport and chemistry;

0322 Atmospheric Composition and Structure: Constituent sources and sinks;

0345 Atmospheric Composition and Structure: Pollution—urban and regional;

Keywords:

hydroxyl radical, hydroperoxyl radical, model comparison, INTEX-A, tropospheric chemistry

1. Introduction

Oxidation chemistry cleanses the atmosphere of chemical emissions from Earth's surface, establishes the global ozone balance, and influences climate change. It is dominated by the hydroxyl radical, OH, but also involves the hydroperoxyl radical, HO_2. OH and HO_2, together called HO_x, are highly reactive atmospheric constituents that have a large impact on the atmospheric chemistry by influencing the removal of gases emitted into the atmosphere and the production of ozone and ultrafine aerosol particles.

The basics of HO_x photochemistry have frequently been described [see for example *Jaeglé et al.*, 2000]. The abundance of OH and HO_2 is primarily influenced by the HO_x production rate, the amount of NO_x (NO_x = NO + NO_2), and to some extent the types of hydrocarbons [*Jaeglé et al.*, 2000; *McKeen et al.*, 1997; *Singh et al.*, 1995; 2003]. In polar regions during springtime, halogen chemistry can influence HO_x and the HO_2/OH ratio in both the marine boundary layer [*Sommariva et al.*, 2005] and the stratosphere [*Hanisco et al.*, 2002].

HO_x has a number of sources: photolysis of O_3 followed by a reaction of $O(^1D)$ with H_2O, photolysis of formaldehyde (HCHO), hydrogen peroxide (H_2O_2), and methylhydroperoxide (CH_3OOH), as well as reactions between O_3 and alkenes. Its destruction is thought to be controlled by the relatively few reactions: HO_2+HO_2, HO_2+OH, HO_2+RO_2, and OH+NO_2. Under high NO_x conditions, HO_x has a heightened sensitivity to HO_x sources [*Olson et al.*, 2006]. Thus, uncertainties in observations and reaction kinetics of HO_x precursors have a much more pronounced impact on modeled HO_x at high NO_x conditions compared to lower NO_x conditions.

The NO_x abundance determines which reactions are the primary HO_x loss. At low NO_x, HO_2 >> OH and the HO_2+HO_2 and HO_2+RO_2 reactions are the primary HO_x loss. As NO_x increases, HO_2+NO→OH+NO_2 increases OH so that the HO_2+OH reaction becomes more

important. At high NO_x, $HO_2+NO \rightarrow OH+NO_2$ cycles even more HO_x to OH and the reaction $OH+NO_2+M \rightarrow HNO_3+M$ becomes the primary loss. As a result, for fixed HO_x production ($P(HO_x)$), OH first increases until NO_x reaches a few ppbv and then decreases as a function of NO_x, while HO_2 remains roughly unchanged until NO_x reaches values for which $OH + NO_2 + M \rightarrow HNO_3 + M$ is the dominant loss and then decreases even faster than OH as NO_x continues to increase. As $P(HO_x)$ increases, the peak OH is higher and shifted to greater NO_x values [*McKeen et al.*, 1997].

Reactions of OH with CO and volatile organic compounds (VOCs) lead to the formation of HO_2 and peroxy radicals (RO_2). This conversion of OH is rapid. The inverse of the OH lifetime, the reaction frequency, which is usually called the OH reactivity, is typically 1 s^{-1} in clean environments and 5-100 s^{-1} in polluted urban environments. At the same time, HO_2 reacts with NO, producing O_3, or with O_3, destroying O_3, and in the process recreates OH. This cycle between OH and HO_2 is at times faster than the production and loss of HO_x. The reaction of RO_2 and NO leads to the formation of HO_2 and NO_2. The exact photochemistry that occurs depends mainly on the HO_x production ($P(HO_x)$), NO_x, the OH reactivity, and the yield of HO_2 and RO_2 from hydrocarbon oxidation [*Kleinman et al,.* 2002]. Understanding HO_x sources, sinks, and cycling is essential to develop predictive capability of pollution's influence on the atmosphere's oxidation capacity.

The ratio of HO_2/OH is an important indicator of the HO_x cycling between OH and HO_2. A steady-state expression for HO_2/OH comes from assuming that OH is in steady-state:

$$\frac{[HO_2]}{[OH]} = \frac{k_{OH}}{\left(k_{NO+HO_2}[NO] + k_{O_3+HO_2}[O_3]\right) + P(OH)_{primary}/[HO_2]} \qquad (1)$$

where $P(OH)_{primary}$ is the OH production rate from either photolysis of long-lived atmospheric constituents or from reactions of O_3 with alkenes; ($k_{NO+HO2}[NO] + k_{O3+HO2}[O_3]$) represents the cycling reaction frequency of HO_x from HO_2 to OH; and k_{OH} is the OH reactivity with all reactants, whether they be HO_x cycling or HO_x terminating reactions. We use the definition for primary OH sources to be those that are independent of local HO_x [*Jaeglé et al.,* 2001]. Typically the photolysis of O_3 followed by $O(^1D)+H_2O$ is the most important OH primary source, although the photolysis of H_2O_2 and CH_3OOH can also be important.

For many atmospheric environments, the primary production, $P(OH)_{primary}$, and the terminating OH reaction rates are much smaller that the rate of reactions that cycle HO_x between OH and HO_2 and can be ignored. However, for the free troposphere between 2 km and 8 km in INTEX-A, the fraction of OH production by $P(OH)_{primary}$ is as often larger than OH production by HO_x cycling, ranging from 0.1 to 0.9, and cannot be ignored.

Because HO_x photochemistry is sufficiently fast, comparisons with box models test the understanding of HO_x photochemistry. While scatter plots of measurements and model calculations are useful, examining the ratio of observed-to-modeled OH and HO_2 as a function of important variables provides even more information. The analyses of airborne tropospheric HO_x measurements from several different studies have been published [e.g., *Wennberg et al.*, 1998; *Crawford et al.*, 1999; *Brune et al.*, 1998; 1999; *Tan et al.*, 2001a; *Olson et al.*, 2004; 2006]. When all of the studies are taken together, we can reach the conclusion that HO_x photochemistry is generally understood to within about a factor of two, but that important larger differences remain for some environments and conditions.

Considering the role of OH and HO_2 in the production of secondary pollutants and the role of OH in the atmosphere's oxidation capacity, a factor of two is far from good enough.

Emerging from HO_x studies are a set of conclusions: (1) HO_2, and thus ozone production, is greater than expected at larger NO values for many tower-based studies and some aircraft studies, even though this discrepancy has been almost eliminated for two previous aircraft studies by reanalyses that more fully account for HO_x precursors and have updated reaction rate coefficients and products [*Olson et al.*, 2006]; (2) HO_2 and OH are larger than expected at high solar zenith angles, as in the Subsonic Assessment: Ozone and Nitrogen Oxide Experiment (SONEX) [*Faloona et al.*, 2000]; (3) the evidence for heterogeneous influence on HO_x is still inconclusive although some studies have provided evidence for significant removal in clouds [*Olson et al.*, 2006]; (4) even with highly constraining measurement suites, OH and HO_2 can be either significantly larger or smaller than expected in different environments and on different missions; whether this variation in agreement is due to unmeasured atmospheric constituents, instrumental drifts and changes, or differences in models, or a combination of all three, is not known; (5) agreement between instruments has been inconsistent from comparison to comparison [*Eisele et al.*, 2001; 2003; *Ren et al.*, 2003].

The Intercontinental Chemical Transport Experiment – A (INTEX-A) was an integrated field experiment performed over North America in summer of 2004. It sought to understand the transport and transformation of gases and aerosols on transcontinental/intercontinental scales and their impact on air quality and climate. A particular focus in this study was to quantify and characterize the inflow and outflow of pollution over North America. The main constituents of interest are ozone and precursors, aerosols and precursors, and long-lived greenhouse gases. Details about the overview and accomplishments of INTEX-A are described by *Singh et al.* [2006]. A broad suite of trace gases including OH and HO_2 radicals and their precursors, aerosols, and meteorological parameters were sampled *in situ* from NASA's DC-8.

The DC-8 encountered a variety of air masses. These include air masses that were influenced by anthropogenic pollution, biomass burning, convection, the stratosphere, and mixtures of these different types. These plumes are often distinguishable by their characteristic composition. Anthropogenic pollution contains high CO, anthropogenic hydrocarbons, and often water vapor. Biomass burning plumes can be distinguished from anthropogenic pollution by high HCN and acetonitrile. Convection plumes can be distinguished by high NO_x/NO_y ratios, water vapor, ultrafine particles, and ozone. Stratosphere-influenced air can be defined as air having O_3 greater than ~100 ppbv, CO less than ~100 ppbv, water vapor less than 200 ppmv, and low hydrocarbon levels. The different composition of these air masses provides an excellent opportunity to examine HO_x photochemistry for a range of conditions.

This paper presents HO_x observation results and a steady state modeling analysis of fast photochemistry using measurements made during the INTEX-A campaign. The HO_x results from INTEX-A are compared to those from previous campaigns and to results for other related measurements from INTEX-A. These analyses provide evidence for the accuracy of the HO_x measurements and for the characteristics of atmospheric processes or constituents that are not incorporated in current models.

2. Experiment and Model Description

2.1 OH and HO_2 Measurements

The OH and HO_2 radicals were measured with the Penn State ATHOS (Aircraft Tropospheric Hydrogen Oxides Sensor). ATHOS detects OH and HO_2 with laser-induced fluorescence (LIF). The technique uses a pump-down technique often called the fluorescent assay by gas expansion (FAGE) originally developed by *Hard et al.* [1984]. A detailed

description of the ATHOS instrument can be found elsewhere [*Faloona et al.*, 2004]; here an abbreviated description of ATHOS is given.

The air sample is drawn into a low-pressure chamber through a pinhole inlet (1.5 mm) with a vacuum pump. The pressure of the detection chamber varied from 12 to 3 hPa from 0 to 12 km altitude. As the air passes through a laser beam, OH is excited by a spectrally narrowed laser with a pulse repetition rate of 3 kHz at one of several ro-vibronic transition lines near 308 nm ($A^2\Sigma$–$X^2\Pi$, v'=0 ← v''=0). Collisional quenching of the excited state is slow enough at the chamber pressure that the weak OH fluorescence extends beyond the prompt scattering (Rayleigh and wall scattering) and is detected with a time-gated microchannel plate (MCP) detector. HO_2 is measured by reaction with NO followed by the LIF detection of OH. The OH and HO_2 detection axes are in series: OH is detected in the first axis and HO_2 in a second axis as reagent NO (>99%, Matheson, Twinsburg, OH, purified through Ascarite) is added to the flow between the two axes. The OH fluorescence signal is detected 60 ns after the laser pulse has cleared in the detection cells and is recorded every 0.2 seconds. The laser wavelength is tuned on and off resonance with an OH transition every 10 seconds, resulting in a measurement time resolution of 20 seconds. The OH fluorescence signal is the difference between on-resonance and off-resonance signals.

The instrument was calibrated both in the laboratory and during the field campaign. Monitoring laser power, Rayleigh scattering, and laser linewidth maintained this calibration in flight [*Faloona et al.*, 2004]. For the calibration, water vapor photolysis by 185 nm light produced OH and HO_2. Absolute OH and HO_2 mixing ratios were calculated by knowing the 185 nm flux, which is determined with a Cs-I phototube referenced to a NIST-calibrated photomultiplier tube from the University of Colorado, the H_2O absorption cross section, the H_2O

mixing ratio, and the exposure time of the H_2O to the 185 nm light. The absolute uncertainty is estimated to be a factor of 1.32 for both OH and HO_2, with a 2σ confidence level. The 2σ precisions during this campaign were about 0.01 pptv for OH and 0.1 pptv for HO_2, with 1 minute integration time. Further details about the calibration process may be found elsewhere [*Faloona et al.*, 2004].

2.2 Other Measurements on the DC-8

The payload of the DC-8 and the measured chemical species and parameters are briefly described in *Singh et al.* [2006]. A large suite of atmospheric constituents were measured in INTEX-A, including CO, O_3, H_2O, reactive nitrogen (NO, NO_2, HNO_3, HO_2NO_2, PAN), more than 50 VOCs and OVOCs, and important HO_x precursors such as peroxides (H_2O_2 and CH_3OOH) and aldehydes (HCHO and acetaldehyde). Spectral radiometers allowed direct measurement of actinic flux used to derive key photolysis frequencies.

During INTEX-A, NO was measured by a commercial NO-NO_x analyzer (Model TEI 42C) based on the chemiluminescence technique because of problems with the primary NO instrument. The commercial NO-NO_x analyzer was operated in NO only mode. A separate *in situ* NO calibration system aboard the DC-8 was used for frequent NO span and background checks. The detection limit of this instrument was about 50 pptv with 1 minute integration time. Due to this relatively high detection limit, measurements of NO_2 were used to constrain the model rather than using measurements of NO. Predictions of NO proved to be generally in good agreement with measurements. A linear regression of the NO obtained from measurements and the model is the equation: $NO_{modeled} = 0.92 \times NO_{measured} - 16$ pptv, with $R^2 = 0.76$. This gives confidence that NO from the model can be used at low NO, where the NO measurement is noisy and may have a

small offset, and at high NO, where NO obtained from measurements and from the model are in excellent agreement.

2.3 Model Description

A zero-dimensional, time-dependent photochemical box model developed at NASA Langley Research Center was used to calculate OH, HO_2 and other reactive intermediates. The model has been described in detail in several previous studies [e.g., *Crawford et al.*, 1999; *Olson et al.*, 2004]. The modeling approach is based on the assumption of a diurnal steady state, which means that the model is integrated in time until the diurnal variation for all calculated species no longer changes from day-to-day. For input, model calculations use observations from the 1-min merged data set available on the INTEX-A public data archive (ftp://ftp-air.larc.nasa.gov/pub/INTEXA/). The minimum set of input constraints includes observations of O_3, CO, NO_2, NMHC, acetone, methanol, temperature, H_2O (dew/frost point), pressure, and photolysis frequencies. For this analysis, analyzed data were limited to solar zenith angles (SZA) between 0˚ and 85˚.

In addition to the required constraints described above, the model has the option to include additional constraints when measurements are available for hydrogen peroxide (H_2O_2), methyl hydrogen peroxide (CH_3OOH), nitric acid (HNO_3), and peroxy acetyl nitrate (PAN). If unavailable, these atmospheric constituents are calculated by the model based on diurnal steady state. While each of the H_2O_2, CH_3OOH, HNO_3, or PAN measurements are missing for 20%-35% of the measurement times, the full suite is missing less than 2% of the measurement times. Model calculations taking advantage of these additional constraints are referred to as "constrained." For the purpose of model-to-measurement comparisons, an unconstrained version

was also run for which none of the additional constraints were exercised; i.e., the peroxides, PAN, and HNO3 were always predicted.

Neither the unconstrained model nor the constrained model was constrained to the measured HCHO, just as was done for previous campaigns. Rather, HCHO is used as an additional species for which comparisons between the observations and model may provide insight into current knowledge of photochemical cycling. Evidence suggests that the differences in the observed and modeled HCHO do not influence the comparisons between observed and modeled OH, HO_2, and HO_2/OH [*Olson et al.*, 2004]. The HO_x results described in this manuscript do not correlate with the deviations between the observed and modeled HCHO.

In order to maximize the number of points available for modeling, nonmethane hydrocarbons were interpolated between consecutive grab samples, which were collected throughout each flight at a frequency of every 4-5 minutes during horizontal flight legs and every 1-2 minutes during ascents and descents. Similarly, acetone and methanol were interpolated between adjacent measurements to fill data gaps.

As in previous studies, photolysis frequencies were based on spectroradiometer measurements [*Shetter and Muller*, 1999]. The diurnal profile for each photolysis frequency is based on clear-sky model calculations using a DISORT eight-stream implementation of the NCAR Tropospheric Ultraviolet Visible (TUV) radiative transfer code [*Madronich and Flocke*, 1998]. The clear-sky diurnal variation from TUV is then normalized to measured photolysis frequencies at the time of observation. Unmeasured photolysis frequencies were first calculated for clear sky conditions and then corrected for ambient cloud conditions based on the ratio of measured-to-calculated photolysis frequency of NO_2.

The uncertainties in the modeled OH and HO_2 are based on the combined uncertainties of the kinetic rate coefficients, the measured chemical concentrations, and the measured and calculated photolysis frequencies. The uncertainties in the model due to kinetic rate constant uncertainties were estimated with a Monte Carlo approach [*Thompson and Stewart*, 1991; *Carslaw et al.*, 1999]. The 2σ uncertainty was estimated to be ±59% for OH and ±53% for HO_2 in the upper troposphere, and ±28% for OH and ±24% for HO2 in the boundary layer.

3. Observations, Model Results, and Comparisons

3.1 HO_x Observations and Comparison with the Model Calculations

Altitude profiles of observed OH and HO_2 spanned from a few hundred meters above the surface to almost 12 km (Figure 1). Median OH was relatively constant at 0.2 pptv from altitudes near the surface to 6 km, but then increased with altitude above 6 km, achieving a maximum of about 0.5 pptv at 12 km. HO_2 decreased as the altitude increased, with a maximum median of ~20 pptv near the surface and a minimum median of ~5 pptv at the highest altitude. The greatest HO_2, almost 60 pptv, was observed just above the surface over the central United States. The median HO_2/OH ratio dropped from 120 near the surface to 12 above 10 km, driven by both the decrease in HO_2 and the increase in OH with altitude. At low altitudes, the spread in HO_2/OH is quite large – from 20 to 300 – indicating a wide range of air composition there.

Overall comparisons of observed and modeled OH and HO_2 show that on average observed OH and HO_2 are less than modeled OH and HO_2, but at lower HO_x mixing ratios, observed OH and HO_2 generally exceeded the modeled OH and HO_2 (Figure 2). For the smallest HO_x values, the observed HO_x exceeds the modeled HO_x by more than the combined 1-σ uncertainties of the model and observations. However, for larger HO_x values, the modeled HO_x

exceeds the observed HO_x by more than the combined 1-σ uncertainties. Because the lower HO_x mixing ratios were mostly observed at high altitudes, these plots suggest that the behavior of HO_x should be investigated as a function of altitude.

Detailed statistics characterize the behavior of the observed-to-modeled ratios as a function of altitude for OH, HO_2, and HO_2/OH (Table 1). The "% within ±32%" is the percentage of model values that are the same as the measured values to within the measurement 2σ uncertainty, the "% mod>obs x 1.32" is the percentage of model values greater than 1.32 times the observed values, and the "% mod<obs/1.32 is the percentage of model values less than the observed values divided by 1.32. Although the model also has uncertainty, using the 2σ measurement uncertainty provides a good indication of the differences between the observed and modeled values and where they are occurring.

OH is generally over-predicted by the model at all altitudes, with roughly two-thirds of the modeled values exceeding observations by more than the 2σ measurement uncertainty (±32%) (Table 1, Figure 3). The large over-prediction of OH is not specific to this model, but is seen with other models as well [*Hudman et al.*, 2006]. For a smaller number of observations, OH is under-predicted in continental boundary layer and in a few plumes at higher altitudes. The under-prediction in the boundary layer correlates strongly with isoprene and will be discussed in detail later.

HO_2 is generally over-predicted below 8 km but is generally under-predicted above 8 km (Table 1, Figure 4). The over-prediction is not as great as for OH and the percentage of modeled values exceeding 1.32 x observed values is less. Large under-predictions of HO_2 in the upper free troposphere above 8 km are highly correlated with NO and will be discussed in detail later.

The HO_2/OH ratio is generally under-predicted throughout the troposphere (Table 1, Figure 5). Below 8 km, the median observed-to-modeled ratio is less than 1.2, close to but slightly exceeding the 2σ uncertainty of the relative measurements of HO_2 and OH, which is ~15%. Median values of the HO_2/OH observed-to-modeled ratio is biased slightly high since OH over-predictions are more severe than those for HO_2. Above 8 km, the large differences in the observed-to-modeled HO_2/OH are driven more by the differences in observed-to-modeled HO_2 than they are in the differences between the observed-to-modeled OH.

3.2 Comparisons of Observed and Modeled HO_x with Previous Studies

ATHOS has measured OH and HO_2 during several recent field studies. The three most recent are the Pacific Exploratory Mission Tropics – B (PEM-TB) [*Raper et al.*, 2001], TRACE-P [*Jacob et al.*, 2003], and INTEX-A [*Singh et al.*, 2006]. PEM-TB was conducted in the tropical Pacific, usually in relatively clean air. In contrast, TRACE-P was conducted off the coast of Asia in air that was often quite polluted. Both occurred in spring and provide an interesting contrast to INTEX-A, which was conducted either over the continental US or over the Atlantic Ocean downwind of it in summer. Comparisons of these three studies are particularly compelling because ATHOS was used to measure OH and HO_2 in all three and OH, HO_2, and HCHO for several previous missions including PEM-TB and TRACE-P were recently recalculated using the same photochemistry and constraints as were used for INTEX-A [*Olson et al.*, 2006].

The behavior of atmospheric constituents that interact with OH and HO_2 is quite different for the three studies (Figure 6). Carbon monoxide (CO) is similar for TRACE-P and INTEX-A, except at lower altitudes where Asian pollution observed during TRACE-P contained much more CO than North American pollution observed during INTEX-A did. CO in both northern

hemisphere studies are roughly twice that observed in PEM-TB. Ozone (O_3) is similar for INTEX-A and TRACE-P up to ~8 km, where O_3 in INTEX-A continues to increase. O_3 in PEM-TB is less than half these other two studies. The greatest differences were with NO_x. Observed NO_x was more than four to five times larger during INTEX-A than during TRACE-P and more than an order of magnitude larger than during PEM-TB. These differences are most pronounced above 8 km, where NO_x during INTEX-A was sometimes more than 1.5 ppbv.

The conditions among the three studies are so different. It is therefore instructive to compare not only the absolute values of OH, HO_2, and the HO_2/OH ratio, but also the ratios of the measured-to-modeled OH, HO_2, and HO_2/OH ratio for the three studies. These are plotted as a function of the controlling environmental factors such as altitude (Figures 3, 4, and 5) and NO (Figure 7).

3.2.1 Comparison as a Function of Altitude

The median observed-to-modeled OH ratio in INTEX-A is similar to that observed in TRACE-P. On the other hand, the median observed-to-modeled OH ratio in INTEX-A is quite different from that in PEM-Tropics B, where it was ~0.6 only below 1 km; above that, the median observed-to-modeled OH ratio increases monotonically to 1.3 at 12 km.

The observed-to-modeled HO_2 ratio has quite different behavior as a function of altitude in INTEX-A compared to that in either TRACE-P or PEM-TB. For altitudes below 8 km, the observed-to-modeled HO_2 ratio is similar for INTEX-A and TRACE-P, both being less than 1, whereas the observed-to-modeled HO_2 ratio was close to 1 for PEM-TB. In all three studies, the ratio changed little over this altitude range. The large increase in the observed-to-modeled HO_2 ratio above 8 km is quite different from either TRACE-P or PEM-TB. This difference is

consistent with the substantially greater NO_x observed above 8 km during INTEX-A than during the other two studies.

Enhanced NO_x was also observed during SUCCESS (Subsonic aircraft; Contrails and Clouds Effect Special Study), both in and out of aircraft exhaust plumes. The ability to conclusively analyze the observations made in the exhaust plumes was limited by sampling with insufficient resolution to appropriately model nonlinear HO_x-NO_x interactions [*Olson et al.*, 2006]. For the SUCCESS observations not impacted directly by aircraft exhaust, a tendency for significant deviation between modeled and observed HO_2 remains [*Brune et al,* 1998]. However, the lack of measurements of several potentially important HO_x precursors limits what can be said with confidence about the under-predicted HO_2 that was observed during SUCCESS.

Similar behavior was observed during TRACE-P, where a subset of the TRACE-P observations in stratospherically influenced air above 9 km near 35^{o}N had an observed-to-modeled HO_2 ratio of 1.6 [*Olson et al.*, 2004]. However, unlike TRACE-P, where the observed-to-modeled ratio was significantly greater than 1 only in stratospherically influenced air, 92% of the INTEX-A observations with an observed-to-modeled HO_2 ratio significantly greater than 1 were in tropospheric air that was not obviously influenced by the stratosphere. Thus this INTEX-A result appears to be unprecedented.

The behavior of the observed-to-modeled HO_2/OH ratio is different in all three studies. For PEM-TB, the observed-to-modeled ratio near 1 at lower altitudes, but above 6 km begins to decrease, reaching 0.6 near 12 km. For TRACE-P, the opposite occurs; the ratio is slightly below 1 at low altitudes, but then increases to about 1.4 above 7 km. The INTEX-A observed-to-modeled HO_2/OH ratios greater than 2 at altitudes above 8 km were not observed in the other

studies. The large increase in the observed-to-modeled HO_2/OH ratio at altitudes above 8 km is driven more by the under-predicted HO_2 rather than the over-predicted OH.

3.2.2 Comparison as a Function of NO

Both OH and HO_2 qualitatively show the expected behavior as a function of NO for INTEX-A (Figure 7), although important quantitative differences occur. For OH, the observed-to-modeled ratios for PEM-TB, TRACE-P, and INTEX-A are fairly constant with increasing NO, even though they are less than 1 for TRACE-P and INTEX-A. In the cleanest conditions, the ratios are close to 1 for both PEM-TB and TRACE-P. The two ratios then diverge until NO ~100 pptv, where they once again converge. Interestingly, for PEM-TB, the observed-to-modeled OH ratio of ~0.6 that occurs for NO > 100 pptv came from only a few hours of observations on one flight when the DC-8 was downwind of recent convection over the Pacific Ocean. These few measurements provide additional evidence that the chemistry associated with convection may be responsible for over-predicted OH in the free troposphere.

The observed-to-modeled HO_2 ratio increases from values below and near 1 to values more than 1 when NO is more than a few hundred pptv in all three studies, although the amount of change is different for the three studies. It is worth noting that the highest NO values were observed in the upper troposphere during INTEX-A, while the highest NO values were observed in boundary layer during TRACE-P.

3.3 HO_x Budget Calculations

Examining the HO_x production and loss provides information about the balance between HO_x sources and sinks. The HO_x production consists of the production from the following

processes: O_3 photolysis followed by the $O(^1D)+H_2O$ reaction, HCHO photolysis (the radical-produced pathway only), H_2O_2 photolysis, and the ozonolysis of alkenes. HO_x loss includes the OH reaction with NO_2 and the reactions among OH, HO_2 and RO_2. For this discussion, RO_2 was calculated by the box model.

The main $P(HO_x)$ was the reaction O^1D+H_2O below 7 km and the photolysis of HCHO above 7 km (Figure 8(a)). Photolysis of H_2O_2 did not contribute much to $P(HO_x)$. For the HO_x loss, HO_2-RO_2 self-reactions were the main processes below 8 km and the $OH+NO_x$ reactions became the main loss processes above 8 km (Figure 8(b)).

3.4 Diurnal Average of Calculated Ozone Production

The net ozone production in the troposphere is given to a close approximation by

$$P(O_3)_{net} = P(O_3) - L(O_3) = k_{NO+HO2}\,[NO][HO_2] + \Sigma_i\, k_{NO+RO2i}\,[NO][RO_{2i}] - k_{OH+NO2+M}\,[M][NO_2][OH] - k_{O1D+H2O}[O(^1D)][H_2O] - k_{HO2+O3}\,[O_3][HO_2] - k_{OH+O3}[O_3][OH] \quad (2)$$

where k_{NO+HO2}, $k_{NO+RO2i}$ $k_{OH+NO2+M}$, $k_{O1D+H2O}$, k_{HO2+O3}, and k_{OH+O3} are reaction rate coefficients. The diurnally averaged values of the ozone production and loss terms come from the time-dependent model simulations. In order to determine the O_3 budget based on observed values of HO_x, the model was run with the computed diurnal profiles of OH and HO_2 scaled throughout the diurnal cycle to match the observed concentrations at the appropriate time of day. The resulting calculated O_3 production was mainly from the HO_2 + NO reaction, especially at altitudes greater than 5 km (Figure 9 (a)). At altitudes around 10 km, the O_3 production from RO_2+NO accounted for less than 10% of the total. For the O_3 loss rate, O_3 photolysis followed

by the $O(^1D) + H_2O$ reaction was the main O_3 loss process below 5 km, while O_3 reactions with OH and HO_2 became the main O_3 loss above 6 km because of low H_2O mixing ratios at these altitudes (Figure 9(b)).

Net calculated ozone production with a median value of 1.3 ppbv d^{-1} was found for the lowest altitude, while a median loss of 1.3 ppbv d^{-1} was found for the lower troposphere (1-5 km). For observations above 9 km, a median net O_3 production rate of 7.0 ppbv d^{-1} was calculated (Figure 9(c)). For the upper altitudes, the O_3 production drops to 4.5 ppbv d^{-1} when model predictions of HO_x are used rather than observed values. This significant difference underscores the importance of understanding the upper tropospheric HO_x discrepancies in the INTEX-A data. The important role of lightning NO_x is also emphasized by the large rates of net production in INTEX-A compared to previous campaigns. Ozone production in the upper troposphere during TRACE-P was less than 1.5 ppbv d^{-1} [*Davis et al.*, 2003] and was ~0.5 ppbv d^{-1} during PEM-Tropics B [*Olson et al.*, 2001].

4. Discussion

Disagreements between observed and modeled HO_x can be caused by instrument error, missing or incorrect chemistry in the model, instrument errors for measurements that are crucial for modeling HO_x, or unmeasured atmospheric constituents that strongly influence HO_x. This situation is complicated by the possibility of changing instrument calibrations and operation and model revisions. As a result, comparisons of measured and modeled HO_x should be examined continually for evidence of discrepancies with either the measurements or the models and for clues to the causes of those discrepancies.

Three significant differences between observed and modeled HO_x become apparent in the INTEX-A data: over-predicted OH throughout the troposphere, with over-predicted HO_2 below 8 km; under-predicted HO_2 above 8 km; and under-predicted OH in the continental planetary boundary layer.

4.1 Over-predicted OH throughout the troposphere

OH was generally over-predicted through the troposphere; HO_2 was generally over-predicted below 8 km. If the observed-to-modeled OH ratios, which were ~0.6 for TRACE-P and INTEX-A and ~1.0 for PEM-TB, are representative and the OH observations are correct, then they suggest that unknown chemistry is suppressing OH throughout the free troposphere in northern midlatitudes. An implication of this over-prediction is that current modeled atmospheric oxidation rates would be too high and the lifetimes of long-lived atmospheric gases like methane and methyl chloroform would be greater than currently thought. Even if OH is suppressed in only the northern midlatitudes, the lifetimes of medium-to-short-lived atmospheric constituents associated with midlatitude emissions would be significantly lengthened, thus allowing transport to have a greater role in determining their distributions.

A concern is that the less-than-expected observed OH and HO_2 comes from an error in the instrument calibration. However, the OH and HO_2 generated by our calibration system is the same to within 10% as the OH and HO_2 generated by the independent calibration systems of two other research groups [*Ren et al.*, 2003; G. Huey, private communication, 2006]. ATHOS has no absolute in-flight calibration, but several monitors and periodic in-flight diagnostics ensure that the calibration is known in flight. It is possible that the angle of air entering the sampling inlet during flight is not being well simulated during the calibration. However, all laboratory and in-

flight diagnostics indicate that the calibration is not sensitive to the angle or velocity of the sampled airflow over the range encountered in flight [*Faloona et al.*, 2004]. We have found no evidence that the observed-to-modeled HO_x differences come from an error in the instrument calibration.

That median observed HO_2 was only 0.78 of modeled HO_2 and median observed OH was only 0.60 of modeled OH has two implications. First, total hydrogen oxides, HO_x ($HO_x = HO_2 + OH$) are either being reduced by an unknown HO_x loss or have a production rate, $P(HO_x)$, that is smaller than calculated. Second, the observed-to-modeled HO_2/OH ratio of ~1.2 indicates that the balance between OH and HO_2 is also being affected.

The observed and modeled HO_x can be brought into agreement by $P(HO_x)$ that is smaller than calculated if the dominant HO_x source, O_3 photolysis followed by $O(^1D)+H_2O$ (Figure 8), is less than calculated by about a factor of two. Such a large difference is not consistent with uncertainties in the measurements of photolysis frequencies, O_3, and H_2O and with many other studies in which O_3 photolysis followed by $O(^1D)+H_2O$ is the primary OH source and good agreement is obtained between observed and modeled OH. Thus, greater-than-expected HO_x loss is the most likely cause.

Consider three possibilities for additional HO_x loss: the rate coefficient for $HO_2+HO_2 \rightarrow H_2O_2+O_2$ is larger than the accepted value; HO_2+RO_2 reactions are faster or RO_2 is greater than calculated; or the amount, number, or reaction rate coefficients for atmospheric constituents that react with OH to terminate HO_x (and not merely cycle to HO_2) are greater than currently known.

A test for errors in the rate coefficient is possible for $HO_2+HO_2 \rightarrow H_2O_2+O_2$ because of two independent hydrogen peroxide measurements that were on the DC-8. The reaction

$HO_2+HO_2 \rightarrow H_2O_2+O_2$ is the only known gas-phase atmospheric H_2O_2 source. The predominant H_2O_2 losses are by reaction with OH and by photolysis. The steady-state equation shows the dependence of steady-state H_2O_2 on HO_2:

$$[H_2O_2]_{ss} = \frac{k_{HO_2+HO_2}[HO_2]^2}{J_{H_2O_2} + k_{H_2O_2+OH}[OH]} \quad (3)$$

where J_{H2O2} is the photolysis frequency for H_2O_2. H_2O_2 may very well not be at steady state because the H_2O_2 photochemical lifetime is approximately 20 sunlit hours, steady state is achieved in about 5 days, H_2O_2 can be injected into the middle and upper troposphere by convection, and H_2O_2 is readily taken up by cloud drops and may react with other dissolved gases in the cloud drops. Even for the unconstrained diurnal steady state model, which is based on HO_x and peroxide concentrations achieving the same values over a 24-hour period, H_2O_2 may not achieve steady-state.

Despite this caveat, the unconstrained model matches the observed H_2O_2 from 1 to 8 km (Figure 10). Confidence in the H_2O_2 measurements is high because the two H_2O_2 measurements agree, on average, to within 10% from 100 pptv to 5000 pptv. In addition, the instantaneous steady-state calculation (see Equation (3)) using the observed HO_2 and OH is a factor of 1.7 lower but has the same behavior with altitude as the observed H_2O_2. This difference is just at the limit of the 2σ absolute uncertainty of the HO_2 and OH measurements propagated through the steady-state equation (Equation 3). The agreement between the observed and modeled H_2O_2 to well within measurement uncertainties for much of the troposphere is strong evidence that an error in the rate coefficient for $HO_2+HO_2 \rightarrow H_2O_2+O_2$ is not the cause of the over-predicted HO_x.

The second possibility – under-predicted RO_2 or errors in the RO_2 rate coefficients – is more difficult to test because RO_2 was not measured on the DC-8 in INTEX-A. In order to account for the HO_2 observed-to-modeled ratio, $k_{HO2+CH3O2}[CH_3O_2]$ would need to be more than 4 times larger than calculated by the model and other $k_{HO2+RO2}[RO_2]$ would need to be approximately 30 times larger. This large increase in CH_3O_2 or RO_2 or their reaction rate coefficients with HO_2 is inconsistent with the hydrocarbon measurements. Some additional evidence is provided by the reasonable agreement between modeled and observed HCHO, which is the dominant intermediate resulting from the oxidation of most hydrocarbons and an indication of the integrated impact of hydrocarbon oxidation [A. Fried, manuscript in preparation]. Thus, this possibility seems as unlikely as the first one.

The third possibility – OH reactions accounting for extra HO_x loss – requires the candidate reaction to be a termination reaction for HO_x (i.e., no subsequent HO_2 or peroxy radical formation). To find the needed additional OH reactivity, OH reactivity was added to the model until the modeled OH agreed with the observed OH for each 1-minute data point. The additional OH reactivity required to bring observed and modeled OH into agreement decreases from almost 1 s^{-1} near the surface to 0.2 s^{-1} at 6 km and then decreases further to less than 0.1 s^{-1} above 10 km (Figure 11). It is about 0.7 of the calculated OH reactivity from other known losses below 6 km and 0.2 above 6 km, both rather large increases in total OH reactivity.

This additional reactivity has an impact on the agreement between observed and modeled HO_2 and thus between the observed and modeled HO_2/OH ratio (Table 2).

The agreement between the observed and modeled HO_2 is dramatically improved in both the middle and lower and troposphere when compared to the agreement without the added OH reactivity as in Table 1. Since OH is forced to agree with observations in these calculations, these

statistics also apply to the HO_2/OH ratio. For the upper troposphere above 8 km, agreement actually worsens, but this is expected since HO_2 was already under-predicted at these altitudes. Thus an additional OH termination reaction could account for the over-prediction of HO_2 and HO_2/OH in the lower and middle troposphere as well as that of OH throughout the troposphere.

What could be the identity of the atmospheric constituent that has under-predicted OH reactivity? Although we do not know its identity, we can identify some of its characteristics. First it is widely distributed throughout the troposphere. Second, its mixing ratio or reaction rate coefficient, which may be temperature dependent, must decrease with height. Third, it appears in both clear and cloud regions and does not correlate with particle surface area density or volume density. Fourth, if its reaction rate coefficient is 2×10^{-12} cm^3 $molecule^{-1}$ s^{-1}, then its mixing ration will be about 20 ppbv near Earth's surface and 2 ppbv above 10 km. Finally, if the difference between the observed-to-modeled HO_x in the northern midlatitudes and in the tropics is not an instrument artifact, then it does not occur in the tropics. We are searching for an atmospheric constituent that has these characteristics.

4.2 Under-predicted HO_2 above 8 km Altitude

Convection had a large impact on the atmospheric composition in this altitude range during INTEX-A [*Bertram et. al.*, 2006), most notably with enhancements in lightning NO_x (Figure 6), but also for peroxides (Figure 10), and sometimes other constituents. Above 8 km, more than 2/3 of the observations of HO_2 and HO_2/OH were greater than expected, while only a small number of OH observations were. As noted above, attempts to reconcile OH at this altitude only worsen comparisons between model and observed HO_2 and HO_2/OH above 8 km.

Could this under-predicted HO_2 be an instrument artifact? An offset to the HO_2 signal would make HO_2 appear larger than it is. However, the observed-to-modeled HO_2 ratio is uncorrelated with observed HO_2, which varied from 2 pptv to 20 pptv above 8 km. In addition, no single offset HO_2 value can be found to improve the agreement between the observed and modeled HO_2. These results rule out a constant offset in the HO_2 signal. The only gas that is known to photolyze in the ATHOS laser beam to produce HO_2, but no OH, is formaldehyde, but the HCHO measured in INTEX-A is orders of magnitude too small to produce the observed signals.

It is interesting that the steady-state H_2O_2 based on the observed HO_2 has the same variation with altitude as the observed H_2O_2, even though the observed H_2O_2 is 1.7 times larger than the steady state value (Figure 10). At altitudes above 8 km, the observed H_2O_2 becomes more than five times larger than the H_2O_2 calculated with the unconstrained model, unlike below between 1 and 8 km where observed and modeled H_2O_2 agree.

The large underestimation of H_2O_2 by the box model above 8 km relates to the possible influence of convective transport. As already noted, convective influence was widespread during INTEX-A. While the lightning NO_x associated with convection would be expected to inhibit the formation of H_2O_2, convective transport could sustain a small background for H_2O_2 in the upper troposphere. Indeed, median H_2O_2 above 8 km is more than an order of magnitude less than median values in the lowest km (177 pptv vs. 2109 pptv) allowing for the possibility that convective transport could explain upper tropospheric H_2O_2 even after significant scavenging.

This convective transport is corroborated by global CTM calculations for the INTEX-A period from the GEOS-Chem model [*Hudman et al.*, 2006]. Box model calculations based on GEOS-Chem chemical conditions were able to reproduce the OH and HO_2 distributions of

GEOS-Chem, but H_2O_2 is severely under-predicted similar to the INTEX-A observations. This similarity between GEOS-Chem and box model results suggests that the under-prediction of H_2O_2 is not due to chemistry, but rather a physical process (e.g., convective transport) not represented in the box model.

The large observed-to-modeled HO_2 ratio above 8 km is not consistent with observed pernitric acid (HO_2NO_2). If HO_2NO_2 were in steady-state with HO_2 and NO_2, the calculated steady-state value of HO_2 would need to be lower than even the modeled HO_2. This difference is consistent with the possibility of the earlier mentioned termination reaction for OH that actually improves the model-to-observed comparison for HO_2NO_2 [*Kim et al.*, 2006].

If the observed HO_2 is not an instrument artifact, then the under-predicted HO_2 indicates an additional unknown HO_x source or a reduced HO_x sink; the under-predicted HO_2/OH indicates either slower HO_x cycling from HO_2 to OH or faster HO_x cycling from OH to HO_2.

Consider first the under-prediction of HO_2. Either an additional unknown HO_x source or a reduced HO_x sink must be capable of improving the observed-to-modeled HO_2 agreement above 8 km without making the agreement worse at lower altitudes. Thus, the cause of HO_2 under-prediction must be insignificant from 2 to 8 km and must have increasing importance from 8 to 11 km.

If less-than-expected HO_x loss is the cause, then the reduced HO_x would need to be an error in the known termination reactions of OH with NO_2, NO, HNO_3, and HO_2NO_2 because they dominate above 8 km and are insignificant below 8 km (Figure 8). However, for terminal HO_x loss by reaction with NO_x to be the cause of the HO_2 under-prediction, the HO_x loss rate by these reactions would have to be 5 to 8 times less than expected. This difference is well outside

uncertainties for the measured reactants and reaction rate coefficients. Thus, a reduced HO_x sink is unlikely to be the cause of the HO_2 under-prediction.

If under-predicted HO_x production is the cause, then the HO_x source could be either an error in the known HO_x sources or additional unknown HO_x sources. The known, equally dominant HO_x sources in the altitude region are O_3 photolysis followed by $O(^1D)+H_2O$ and HCHO photolysis. In order to bring modeled and observed HO_2 into agreement, an additional HO_x source of $1x10^6$ molecules cm^{-3} s^{-1} is needed above 10 km. This amount is 2-3 times larger than the known HO_x sources (Figure 8). Below 10 km, this source would need to decrease to less than $\sim10^5$ molecules cm^{-3} s^{-1} at 6 km and below. It is worth noting that this increase with altitude of the needed additional HO_x source is similar to the observed increase in NO_x with increasing altitude (Figure 6).

Can the HO_2 under-prediction come from errors in a known source? The O_3 photolysis and HCHO photolysis are about equal HO_x sources above 8 km. The HO_x production rate from either one of them would need to be increased by a factor of 4 to 6 above 10 km. O_3 photolysis could not be low by that much at 10 km and still be consistent with the HO_x observed-to-modeled ratios below 10 km, where O_3 photolysis is the dominant HO_x source. This inconsistency rules out an error in O_3 photolysis as the cause of the HO_2 under-prediction. An error in the HCHO photolysis would have to be in the photolysis frequency because modeled and observed HCHO are in good agreement in the upper troposphere [A. Fried, manuscript in preparation]. It is quite unlikely that the HCHO photolysis frequency could be in error by a factor of 4 to 6. Thus errors in the known HO_x sources are not likely to be the cause of the HO_2 under-prediction.

Thus, unknown HO_x sources are the most likely cause of the HO_2 under-prediction. One characteristic of the unknown source is that it correlates with NO. For the observed-to-modeled HO_2 ratio above 8 km, the HO_2 observed-to-modeled ratio = 0.002 x NO (in pptv) + 0.70 with R^2 = 0.52. In previous studies, it was assumed that the chemistry and HO_x sinks were understood and that the under-predicted HO_2 was due to missing HO_x sources that were emitted along with the NO [see for example *Folkins et al.*, 1997; *Wennberg et al.*, 1998; *Jaeglé et al.*, 2000]. While we have been able to quantify the additional HO_x production that would be needed, to identify its altitude dependence, and to show a correlation with NO, we have not been able to identify this additional unknown HO_x source.

A second issue is the under-predicted HO_2/OH ratio. This ratio indicates that reactions and reactants that cycle HO_x between OH and HO_2 are not being properly represented in the model. The HO_2/OH under-prediction can be explained by either slower reactions of HO_2 with NO or faster OH reactions that cycle OH to HO_2. At these altitudes, the reaction frequency of $HO_2+NO \rightarrow OH+NO_2$ is an order of magnitude faster than primary OH production (Equation 1). The reaction frequency for HO_2+NO would need to be less than ½ its calculated value; this difference is unlikely and inconsistent many other studies. It is possible that other reactants with HO_2, such as BrO, are present, but their reactions with HO_2 would make HO_2/OH smaller, not larger. Thus, the under-predicted HO_2/OH ratio indicates the presence of unknown reactants or reactions with OH that cycle HO_x from OH to HO_2.

In this case, the needed increase in the OH reactivity is proportional to the observed-to-modeled HO_2/OH ratio. As a result, the needed additional OH reactivity is ~0.15 s^{-1} at 8 km, about ½ of the calculated OH reactivity, and ~0.5 s^{-1} above 10 km, almost twice the calculated OH reactivity. Interestingly, the needed OH reactivity is roughly proportional to the increase in

NO_x in that altitude range, suggesting that the convective processes that enhanced NO_x also yielded additional, unknown OH reactants.

Evidence suggests that the cause of the under-predicted HO_x is unrelated to the cause of the under-predicted HO_2/OH ratio. This evidence comes from the differences observed in tropospheric air and stratosphere-influenced air. In the stratosphere-influenced air, the observed-to-modeled OH and HO_2 increase from ~1 at 7 km to ~2 at 10 km before decreasing again to 1 above 11 km (Figure 12). The median observed-to-modeled HO_2/OH ratio, on the other hand, remains very close to 1.0 for the entire altitude range of 7-12 km. This behavior is quite different from that of the tropospheric air at the same altitudes, as shown in Figure 5 and from the TRACE-P observation in stratosphere-influenced air, in which the mean HO_2/OH observed-to-modeled ratio was 1.25 [*Olson et al.*, 2006].

For INTEX-A stratosphere-influenced air, the greatest observed-to-modeled OH and HO_2 ratios occur in dry air that contains over 300 ppbv of ozone. In contrast, the observed-to-modeled ratios for OH, HO_2, and HO_2/OH are all close to 1 for the stratosphere-influenced air observed at 11.5 km. This air was encountered on a flight early over the Pacific Ocean during INTEX-A and may not have been affected by convection recently.

In the presence of greater NO, the differences in OH and HO_2 between the model constrained to observed HNO_3, H_2O_2, CH_3OOH, and HO_2NO_2 and the model unconstrained by these observations grows (Figure 13). This behavior indicates that the modeled OH and HO_2 are quite sensitive to the model constraints, especially above 8 km altitude where the NO was increasing. In this altitude region, the cycling of HO_2 due to NO dominates the primary production of HO_x and makes HO_x more sensitive to small differences in the constraints placed on the model photochemistry.

4.3 Under-predicted OH in the Continental Planetary Boundary Layer

During INTEX-A, the observed-to-modeled OH ratio is frequently much greater than one below 2 km altitude above ground level, in the planetary boundary layer. The location of these large ratios coincides with forested regions where isoprene is abundant, primarily from the Gulf Coast states up through Appalachia and the Midwest. The observed-to-modeled OH ratio is a strong function of isoprene (Figure 14). It increases slowly from 0.6 to 1 as isoprene increases from less than 10 pptv to 500 pptv, but for isoprene levels exceeding 500 pptv, the observed-to-modeled OH ratio rapidly increased to ~3 as isoprene increases.

This observation from INTEX-A is consistent with tower-based observations made with a different configuration of the same instrument. In the summers of 1998 and 2000, OH and isoprene measurements were made on a tower at the PROPHET site in a Michigan forest [*Tan et al.*, 2001b]. The median daytime (SZA < 60^{o}) observed-to-modeled OH ratio depends on isoprene in a way that is consistent with and overlaps the INTEX-A measurements, as seen by the triangles in Figure 14.

The reasons for the higher-than-expected OH at high isoprene levels are not clear, but most likely are due to a missing OH source in the model. For PROPHET, the agreement between observed and modeled OH is improved by introducing additional terpenes that react with O_3 to form OH [*Tan et al.*, 2001b]. In addition, the difference between the observed and calculated OH reactivity is consistent with the emission of unmeasured terpenes that have ratios of O_3 reactions with terpenes that form OH to the OH reactions with terpenes that are similar to that of terpinolene, a sesquiterpene [*DiCarlo et al.*, 2004]. That the under-predicted OH was observed over several forested areas during INTEX-A provides strong evidence that this effect is not

specific only to the PROPHET site in northern lower Michigan, but is, in fact, a more widespread property of the atmospheric chemistry over forests.

5. Summary and Conclusions

Measurements of OH and HO_2 were compared to the model calculations in the INTEX-A summer 2004 campaign. This study provides an excellent opportunity to test oxidation chemistry in pollution plumes throughout the troposphere and the following conclusions can be drawn from this study.

First, for most of the troposphere, observed OH and HO_2 were less than expected from model calculations. On average observed OH was 0.6 of modeled OH and observed HO_2 was 0.78 of modeled HO_2. This observed-to-modeled comparison is similar to that for TRACE-P, another mid-latitude study, but is different from that for PEM-TB, a tropical study, for which observed and modeled HO_2 generally agreed to within a factor of 1.3. In contrast, above 8 km during INTEX-A, the observed-to-modeled HO_2 ratio increased from about 1 at 8 km to about 3 at 11 km.

Second, HO_x budget analysis shows that the main HO_x sources are O_3 photolysis followed by the $O(^1D)+H_2O$ reaction below 7 km and the photolysis of HCHO above 7 km. The main HO_x sinks are the HO_2-RO_2 self-reactions below 8 km and $OH+NO_x$ reactions above 8 km.

Third, O_3 budget analysis shows that the diurnally averaged calculated net O_3 loss rate was 1.3 ppbv d^{-1} at altitudes between 1 and 5 km. Above 9 km, the diurnally averaged calculated net O_3 production rate was 4.5 ppbv d^{-1} using modeled HO_2 and 7.0 ppbv d^{-1} using observed HO_2. This difference between the calculated net O_3 production from the modeled HO_2 and the observed HO_2 is significant and a concern.

Fourth, the under-predicted OH and HO_2 for the two studies in northern midlatitudes - TRACE-P and INTEX-A – and the agreement between observed and modeled OH and HO_2 for a study in the tropics - PEM-TB - suggests the presence of unknown atmospheric constituents or unknown reactions with OH that are suppressing the observed OH throughout much of the troposphere at northern midlatitudes. An unknown reaction or reactant with OH that terminates HO_x and has an OH reactivity comparable to the known OH reactions would improve the agreement between observed and modeled OH and HO_2. If this discrepancy is due to emission sources and not to measurement calibrations and changes in measurements calibrations from study to study, then the lifetime of gases that are destroyed by OH, the atmosphere's oxidation capacity, and the evolution of the atmosphere's oxidation capacity will all need to be re-examined.

Fifth, the under-predicted HO_2 at altitudes above 8 km suggests the presence of an unknown HO_x source or an error in the model's chemistry involving some of the other atmospheric constituents. The consistency in the increase of the observed-to-modeled HO_2 ratio altitude and the increase in NO with altitude suggests that an unknown HO_x source comes from the convective processes that cause the enhanced NO. Evidence from the constrained and unconstrained model runs indicates that OH and HO_2 are particularly sensitive to the NO.

Sixth, the observed-to-modeled OH ratio in the planetary boundary layer in forested regions is a strong function of isoprene. It increases slowly from 0.6 to 1 as isoprene increases from less than 10 pptv to 500 pptv, but for isoprene levels exceeding 500 pptv, the observed-to-modeled OH ratio rapidly increased to ~3. This isoprene dependence of observed-to-modeled OH ratio is consistent with the PROPHET measurements, indicating that this under-predicted OH, if not due to instrument artifacts, occurs in widespread forested regions.

It seems more likely to us that, if the over-predicted OH throughout much of the troposphere and under-predicted HO_2 above 8 km are not measurement artifacts, then their causes are due to unknown atmospheric constituents that are acting as HO_x sources or OH sinks or to unknown reactions and not to large errors in the measurements of either atmospheric constituents or the photochemical rate coefficients. These three major differences between observed and modeled HO_x appear to have different causes.

Because the over-predicted OH throughout the troposphere, under-predicted HO_2 above 8 km, and under-predicted OH above forests have strong implications for understanding global-scale tropospheric oxidation chemistry, finding the causes for these differences should be a high priority. Progress in resolving these discrepancies requires further examination of possible unknown OH sinks and HO_x sources and a focused research activity devoted to ascertaining the accuracy of the OH and HO_2 measurements.

Acknowledgment

The work was supported by the NASA Tropospheric Chemistry Program. The authors would like to thank the DC-8 crew and support staff during the INTEX-A preparation and deployment periods for making this work possible.

References

Bertram, T. H., et al. (2006), Direct measurements of the convective Recycling of the upper troposphere, submitted.

Brune, W. H., et al. (1998), Airborne in-situ OH and HO_2 observations in the cloud-free troposphere and lower stratosphere during SUCCESS, *Geophys. Res. Let.*, 25, 1701–1704.

Brune, W. H., et al., (1999), OH and HO_2 chemistry in the North Atlantic free troposphere, *Geophys. Res. Lett.*, 26, 3077–3080.

Carslaw, N., P. J. Jacobs, and M. J. Pilling (1999), Modeling OH, HO_2, and RO_2 radicals in the marine boundary layer 2. Mechanism reduction and uncertainty analysis, *J. Geophys. Res.*, 104, 30,257–30,273.

Crawford, J., et al. (1999), Assessment of upper tropospheric HO_x source over the tropical Pacific based on NASA GTE/PEM data: Net affect on HO_x and other photochemical parameters, *J. Geophys. Res.*, 104, 16,255–16,273.

Davis, D. D., et al. (2003), An assessment of western North Pacific ozone photochemistry based on springtime observations from NASA's PEM-West B (1994) and TRACE-P (2001) field studies, *J. Geophys. Res.*, 108, 8829, doi:10.1029/2002JD003232.

Di Carlo, P, W. H. Brune, M. Martinez, H. Harder, R. Lesher, X. Ren, T. Thornberry, M. A. Carroll, V. Young, P. B. Shepson, D. Riemer, E. Apel, and C. Campbell (2004), Missing OH reactivity in a forest: evidence for unknown reactive biogenic VOCs, *Science,* 304, 722–725.

Eisele, F. L., R. L. Mauldin, D. J. Tanner, C. Cantrell, E. Kosciuch, J. B. Nowak, B. Brune, I. Faloona, D. Tan, D. D. Davis, L. Wang, and G. Chen (2001), Relationship between OH measurements on two different NASA aircraft during PEM Tropics B, *J. Geophys. Res.*, 106, 32,683–32,689.

Eisele, F. L., et al. (2003), Summary of measurement intercomparisons during TRACE–P, *J. Geophys. Res.*, 108, 8791, doi:10.1029/2002JD003167.

Faloona, I., *et al*. (2000), Observations of HO_x and its relationship with NO_x in the upper troposphere during SONEX, *J. Geophys. Res*., 105, 3771–3783.

Faloona, I. C., D. Tan, R. L. Lesher, N. L. Hazen, C. L. Frame, J. B. Simpas, H. Harder, M. Martinez, P. DiCarlo, X. Ren, and W. H. Brune (2004), A laser-induced fluorescence instrument for detecting tropospheric OH and HO_2: Characteristics and calibration, *J. Atmos. Chem.*, 47, 139–167.

Folkins, I., P. O. Wennberg, T. F. Hanisco, J. G. Anderson, R. J. Salawitch (1997), OH, HO_2, and NO in two biomass burning plumes: Sources of HO_x and implications for ozone production, *Geophys. Res. Let.*, 24, 3185–3188.

Hanisco, T. F., J. B. Smith, R. M. Stimpfle, D. M. Wilmouth, J. G. Anderson, E. C. Richard, and T. P. Bui (2002), In situ observations of HO_2 and OH obtained on the NASA ER-2 in the high-ClO conditions of the 1999/2000 Arctic polar vortex, *J. Geophys. Res.*, 107, 8283, doi:10.1029/2001JD001024.

Hard, T. M., R. J. O'Brien, C. Y. Chan, and A. A. Mehrabzadeh (1984), Tropospheric free radical determination by FAGE, *Environ. Sci. Technol., 18*, 768–777.

Hudman, R. C., et al. (2006), Surface and lightning sources of nitrogen oxides in the United States: magnitudes, chemical evolution, and outflow, submitted to *J. Geophys. Res.*

Jacob, D. J., J. H. Crawford, M. M. Kleb, V. S. Connors, R. J. Bendura, J. L. Raper, G. W. Sachse, J. C. Gille, L. Emmons, and C. L. Heald (2003), Transport and Chemical Evolution over the Pacific (TRACE-P) aircraft mission: Design, execution, and first results, *J. Geophys. Res.*, 108, 9000, doi:10.1029/2002JD003276.

Jaeglé, L., D. J. Jacob, W. H. Brune, I. Faloona, D. Tan, B. G. Heikes, Y. Kondo, G. W. Sachse, B. Anderson, G. L. Gregory, H. B. Singh, R. Pueschel, G. Ferry, D. R. Blake, and R. E. Shetter (2000), Photochemistry of HO_x in the upper troposphere at northern midlatitudes, *J. Geophys. Res.*, 105, 3877–3892.

Jaeglé, L., D. J. Jacob, W. H. Brune, and P.O. Wennberg (2001), Chemistry of HO*x* radicals in the upper troposphere, *Atmos. Environ.*, 35, 469–489.

Kim, S., et al. (2006), Measurement of HO_2NO_2 in the upper troposphere during INTEX-NA 2004, submitted to *J. Geophys. Res.*

Kleinman, L. I., P. H. Daum, Y. -N. Lee, L. J. Nunnermacker, S. R. Springston, J. Weinstein-Lloyd, and J. Rudolph (2002), Ozone production efficiency in an urban area, *J. Geophys. Res.*, 107, 4733, doi:10.1029/2002JD002529.

Madronich, S., and S. Flocke (1998), The role of solar radiation in atmospheric chemistry, in Handbook of Environmental Chemistry, edited by P. Boule, pp. 1–26, Springer, New York.

Martinez, M., et al. (2003), OH and HO_2 concentrations, sources, and loss rates during the Southern Oxidants Study in Nashville, Tennessee, summer 1999, *J. Geophys. Res.*, 108, 4617, doi: 10.1029/2003JD003551.

McKeen, S. A., G. Mount, F. Eisele, E. Williams, J. Harder, P. Goldan, W. Kuster, S. C. Liu, K. Baumann, D. Tanner, A. Fried, S. Sewell, C. Cantrell, and R. Shetter (1997), Photochemical modeling of hydroxyl and its relationship to other species during the Tropospheric OH Photochemistry Experiment. *J. Geophys. Res.*, 102, 6467–6493.

Olson, J. R., et al. (2001), Seasonal differences in the photochemistry of the South Pacific: A comparison of observations and the model results fro PEM-Tropics A and B, *J. Geophys. Res.*, 106, 32,749–32,766.

Olson, J. R. et al. (2004), Testing fast photochemical theory during TRACE-P based on measurements of OH, HO_2, and CH_2O, *J. Geophys. Res.*, 109, D15S10, doi:10.1029/2003JD004278.

Olson, J. R., J. H. Crawford, G. Chen, W. H. Brune, I. C. Faloona, D. Tan, H. Harder, and M. Martinez (2006), A reevaluation of airborne HO_x observations from NASA field campaigns, *J. Geophys. Res.*, 111, D10301, doi:10.1029/2005JD006617.

Raper, J. L., M. M. Kleb, D. J. Jacob, D. D. Davis, R. E. Newell, H. E. Fuelberg, R. J. Bebdura, J. M. Hoell, and R. J. McNeal (2001), Pacific Exploratory Mission in the Tropical Pacific: PEM-Tropics B, March-April 1999, *J. Geophys. Res.*, 106, 32,401–32,425.

Ren, X., H. Harder, M. Martinez, R. L. Lesher, A. Oliger, J. B. Simpas, W. H. Brune, J. J. Schwab, K. L. Demerjian, Y. He, X. L. Zhou, and H. Gao (2003), OH and HO_2 chemistry in the urban atmosphere of New York City, *Atmos. Environ.*, 37, 3639–3651.

Ren, X., G. D. Edwards, C. A. Cantrell, R. L. Lesher, A. R. Metcalf, T. Shirley, and W. H. Brune (2003), Intercomparison of peroxy radical measurements at a rural site using laser-induced fluorescence and Peroxy Radical Chemical Ionization Mass Spectrometer (PerCIMS) techniques, *J. Geophys. Res.*, 108, 4605, doi: 10.1029/2003JD003644.

Shetter, R. E., and M. Muller (1999), Photolysis frequency measurements using actinic flux spectroradiometry during the PEM-Tropics mission: Instrumentation description and some results, *J. Geophys. Res.*, 104, 5647–5661.

Singh, H. B., M. Kandaidou, P. J. Crutzen, and D. J. Jacob (1995), High concentrations and photochemical fate of oxygenated hydrocarbons in the global troposphere. *Nature*, 378, 50–54.

Singh, H. B., W. H. Brune, and J. H. Crawford (2003), Reactive nitrogen and hydrogen in the global atmosphere: Progress in measurements and theory, in *Recent Advances in Atmospheric and Oceanic Sciences-Part-II: Air Pollution Studies*, Proceedings of the Indian National Science Academy, 69/6, 669–683.

Singh, H. B., W. H. Brune, J. H. Crawford, and D. J. Jacob (2006), Overview of the Summer 2004 Intercontinental Chemical Transport Experiment-North America (INTEX-A), submitted to *J. Geophys. Res.*

Sommariva, R., et al. (2005), OH and HO_2 chemistry during NAMBLEX: roles of oxygenates, halogen oxides and heterogeneous uptake, *Atmos. Chem. Phys. Discuss.*, 5, 10,947–10,996.

Spivakovsky, C. M., et al. (2000), Three-dimensional climatological distribution of tropospheric OH: Update and evaluation, *J. Geophys. Res.*, 105, 8931–8980.

Tan, D., et al. (2001a), OH and HO_2 in the tropical Pacific: Results from PEM Tropics B, *J. Geophys. Res., 106*, 32,667–32,681.

Tan, D., I. Faloona, J. B. Simpas, W. Brune, P. B. Shepson, T. L. Couch, A. L. Sumner, M. A. Carroll, T. Thornberry, E. Apel, D. Riemer, and W. Stockwell (2001b), HO_x budgets in a deciduous forest: Results from the PROPHET summer 1998 campaign, *J. Geophys. Res.*, 106, 24,407–24,427.

Thompson, A. M., and R. W. Stewart (1991), Effect of chemical kinetics uncertainties on calculated constituents in a tropospheric photochemical model, *J. Geophys. Res.*, 96, 13,089–13,108.

Wennberg, P. O., et al. (1998), Hydrogen radicals, nitrogen radicals, and the production of O_3 on the upper troposphere, *Science*, 279, 49–53.

Figure captions:

Figure 1. Observed OH and HO_2 mixing ratios and HO_2/OH ratio as a function of altitude during INTEX-A. Small dots are the 1-minute averaged data; the linked circles denote median values in 0.5 km altitude bins.

Figure 2. Comparison of observed and modeled OH (a) and HO_2 (b) for INTEX-A. The straight solid lines indicate the 1:1 lines, the dashed lines indicate the 1-σ uncertainty in the model (±30% for OH and ±27% for HO_2), the solid line with circles are the median values for the observations, and the dash-dot lines are the 1-σ uncertainty for the observations (±16%).

Figure 3. Comparison of the vertical profiles of (left) measured (circles) and modeled (stars) OH for INTEX-A and (right) measured-to-modeled OH ratios in INTEX-A (circles), TRACE-P (stars) and PEM Tropics B (triangles). Individual INTEX-A 1-minute measurements are shown (gray dots).

Figure 4. Comparison of the vertical profiles of (left) measured (circles) and modeled (stars) HO_2 for INTEX-A and (right) measured-to-modeled HO_2 ratios in INTEX-A (circles), TRACE-P (stars) and PEM Tropics B (triangles). Individual INTEX-A 1-minute measurements are shown (gray dots).

Figure 5. Comparison of the vertical profiles of (left) measured (circles) and modeled (stars) HO_2/OH for INTEX-A and (right) measured-to-modeled HO_2/OH in INTEX-A (circles), TRACE-P (stars) and PEM Tropics B (triangles). Individual INTEX-A 1-minute measurements are shown (gray dots).

Figure 6. Comparisons of the altitude profiles for atmospheric constituents for PEM Tropics B (triangles), TRACE-P (stars), and INTEX-A (circles) for (left) CO, (middle) NO_x, and (right) O_3. Individual 1-minute measurements for INTEX-A are shown as gray points.

Figure 7. Comparison of NO dependence for (a) OH and (b) HO_2 of (up) measured (circles) and modeled (stars) values and (down) measured-to-modeled ratios in INTEX-A (circles), TRACE-P (stars) and PEM Tropics B (triangles). Individual INTEX-A 1-minute measurements are shown (gray dots). Concentrations of NO calculated in the model are used in this figure.

Figure 8. Vertical median profiles of (a) HO_x production: total (thick line), from $O(^1D)+H_2O$ (circles), from HCHO photolysis (stars), and from H_2O_2 photolysis (triangles); and (b) HO_x loss rates: total (thick line), due to HO_2+HO_2/RO_2 (circles), due to $OH+HO_2$ (stars), and due to $OH+NO_x$ (triangles) during INTEX-A. Small gray dots show the 1-minute data for (a) total HO_x production rate and (b) total HO_x loss rate. All the production and loss rates were calculated from the measurements, except for RO_2+HO_2 where RO_2 levels were calculated in the model.

Figure 9. Vertical median profiles of (a) instantaneous O_3 production rate: total (circles), from HO_2+NO (stars), and from RO_2+NO (triangles) where RO_2 levels were calculated in the model; (b) O_3 loss rate: total (circles), due to $O(^1D)+H_2O$ (stars), due to O_3+OH (triangles), and due to O_3+HO_2 (solid line); and (c) net O_3 production rate during INTEX-A. Small gray dots show the 1-minute data for (a) total O_3 production rate, (b) total O_3 loss rate, and (c) net O_3 production.

Figure 10. Variation of median H_2O_2 with altitude for the unconstrained instantaneous model (dotted line), the steady-state calculation using observed OH and HO_2 (solid line), and the measurements of the University of Rhode Island (circles) and California Institute of Technology (stars). Steady-state H_2O_2 calculated from observed HO_2 are shown for each minute (gray dots).

Figure 11. Altitude variation of the calculated OH reactivity (grey dots), altitude-averaged calculated OH reactivity (stars), and the additional OH reactivity needed in the model to bring the measured and modeled HO_2 into agreement (circles).

Figure 12. Observed-to-modeled OH, HO_2, and HO_2/OH ratios in stratosphere-influenced air. Shown are 1-km median values (circles and lines) and individual 1-minute values (gray dots).

Figure 13. Ratio of constrained-to-unconstrained models for OH (a) and HO_2 (b) as a function of NO. Individual 1-minute comparisons are presented (gray dots) as well as median values (circles and lines).

Figure 14. The observed-to-modeled OH ratio as a function of isoprene. Individual 1-minute measurements (gray points) and median values for isoprene intervals (circles) are shown for data taken at less than 1 km altitude and solar zenith angle less than 60^o. Median observed-to-modeled OH ratios from the PROPHET tower in a Michigan forest in summer 2000 are also shown (triangles).

Table 1. Statistics for HO_x observed-to-modeled ratios

OH obs/mod	Overall	0-2 km	2-8 km	8-12 km
median (mean)	0.60 (0.79)	0.66 (1.04)	0.57 (.66)	0.60 (0.76)
% within ±32%	18%	18%	17%	19%
% mod<obs/1.32	10%	22%	3%	9%
% mod>obs x 1.32	72%	59%	79%	72%
HO_2 obs/mod	Overall	0-2 km	2-8 km	8-12 km
median (mean)	0.78 (1.75)	0.83 (0.96)	0.69 (1.28)	1.25 (3.35)
% within ±32%	38%	54%	31%	36%
% mod<obs/1.32	16%	11%	<1%	47%
% mod>obs x 1.32	46%	36%	69%	17%
HO_2/OH obs/mod	Overall	0-2 km	2-8 km	8-12 km
median (mean)	1.28 (1.64)	1.17 (1.17)	1.17 (1.22)	2.20 (2.88)
% within ±32%	42%	45%	57%	13%
% mod<obs/1.32	47%	34%	33%	83%
% mod>obs x 1.32	11%	21%	10%	4%

Table 2. Statistics for HO_2 observed-to-modeled ratio with added OH reactivity

HO_2 obs/mod	Overall	0-2 km	2-8 km	8-12 km
median (mean)	1.13 (1.58)	1.08 (1.17)	1.01 (1.10)	2.31 (2.88)
% within ±32%	55%	67%	72%	13%
% mod<obs/1.32	35%	21%	15%	84%
% mod>obs x 1.32	10%	12%	13%	4%

Figure 1. Observed OH and HO_2 mixing ratios and HO_2/OH ratio as a function of altitude during INTEX-A. Small dots are the 1-minute averaged data; the linked circles denote median values in 0.5 km altitude bins.

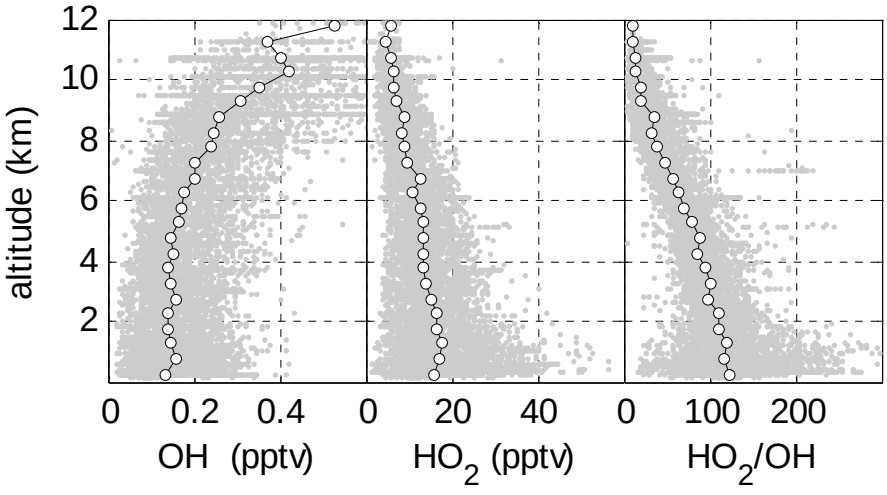

Figure 2. Comparison of observed and modeled OH (a) and HO_2 (b) for INTEX-A. The straight solid lines indicate the 1:1 lines, the dashed lines indicate the 1-σ uncertainty in the model (±30% for OH and ±27% for HO_2), the solid line with circles are the median values for the observations, and the dash-dot lines are the 1-σ uncertainty for the observations (±16%).

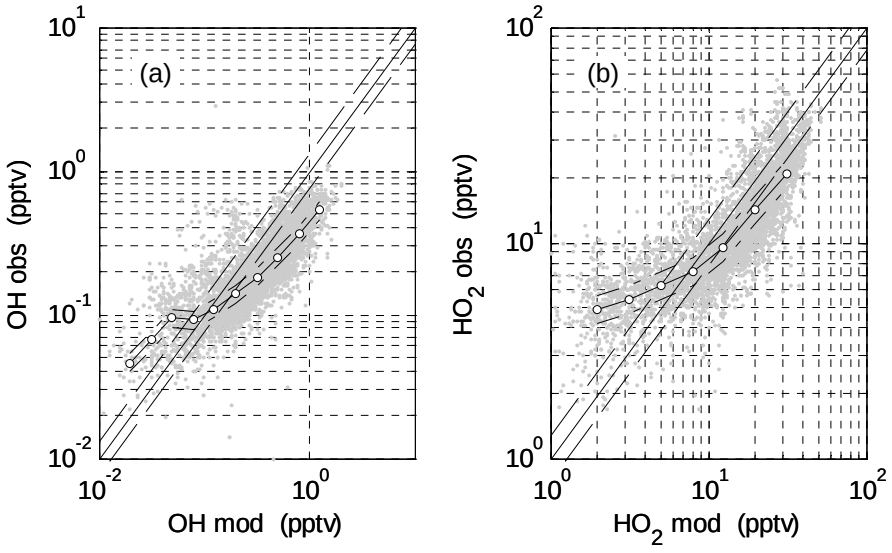

Figure 3. Comparison of the vertical profiles of (left) measured (circles) and modeled (stars) OH for INTEX-A and (right) measured-to-modeled OH ratios in INTEX-A (circles), TRACE-P (stars) and PEM Tropics B (triangles). Individual INTEX-A 1-minute measurements are shown (gray dots).

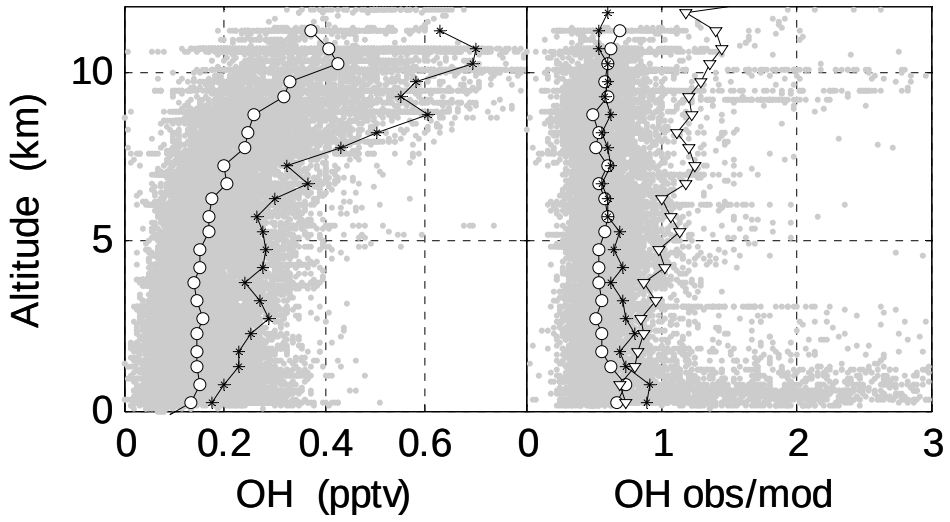

Figure 4. Comparison of the vertical profiles of (left) measured (circles) and modeled (stars) HO_2 for INTEX-A and (right) measured-to-modeled HO_2 ratios in INTEX-A (circles), TRACE-P (stars) and PEM Tropics B (triangles). Individual INTEX-A 1-minute measurements are shown (gray dots).

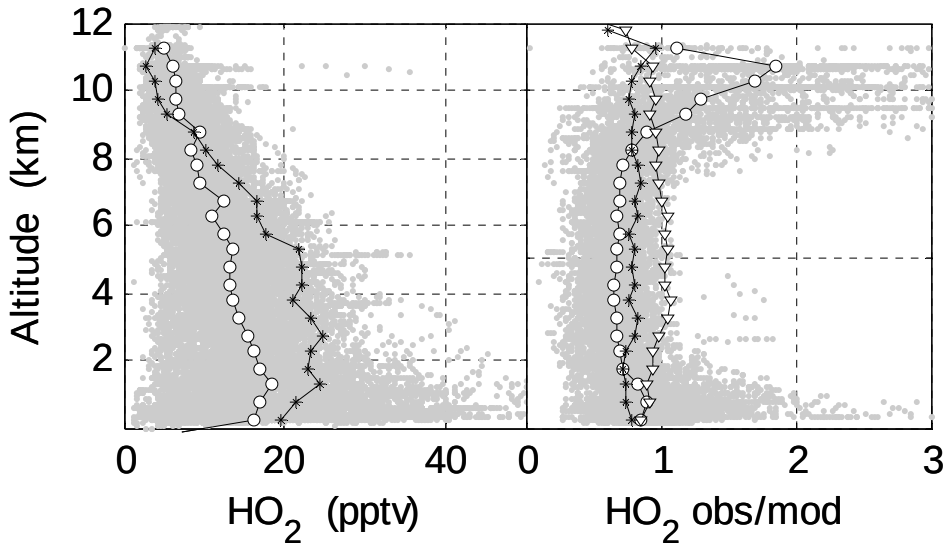

Figure 5. Comparison of the vertical profiles of (left) measured (circles) and modeled (stars) HO_2/OH for INTEX-A and (right) measured-to-modeled HO_2/OH in INTEX-A (circles), TRACE-P (stars) and PEM Tropics B (triangles). Individual INTEX-A 1-minute measurements are shown (gray dots).

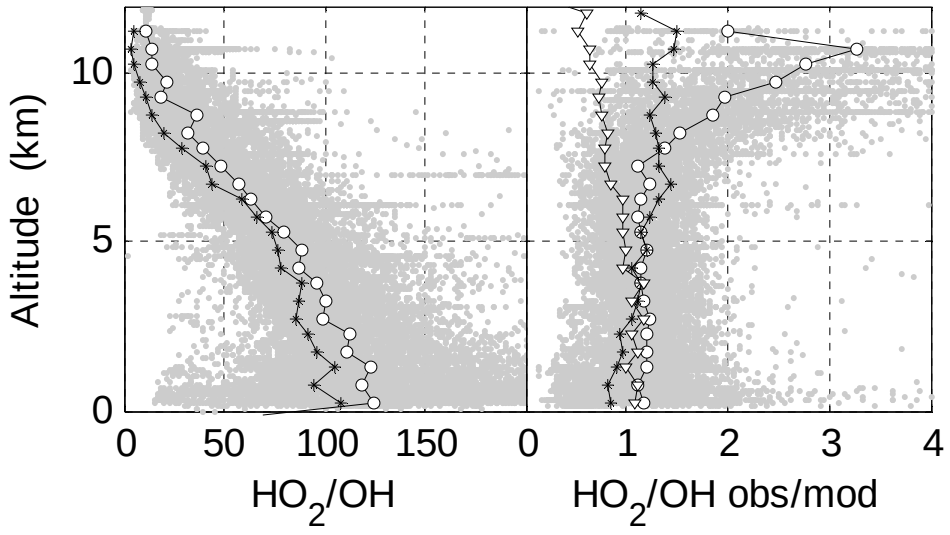

Figure 6. Comparisons of the altitude profiles for atmospheric constituents for PEM Tropics B (triangles), TRACE-P (stars), and INTEX-A (circles) for (left) CO, (middle) NO_x, and (right) O_3. Individual 1-minute measurements for INTEX-A are shown as gray points.

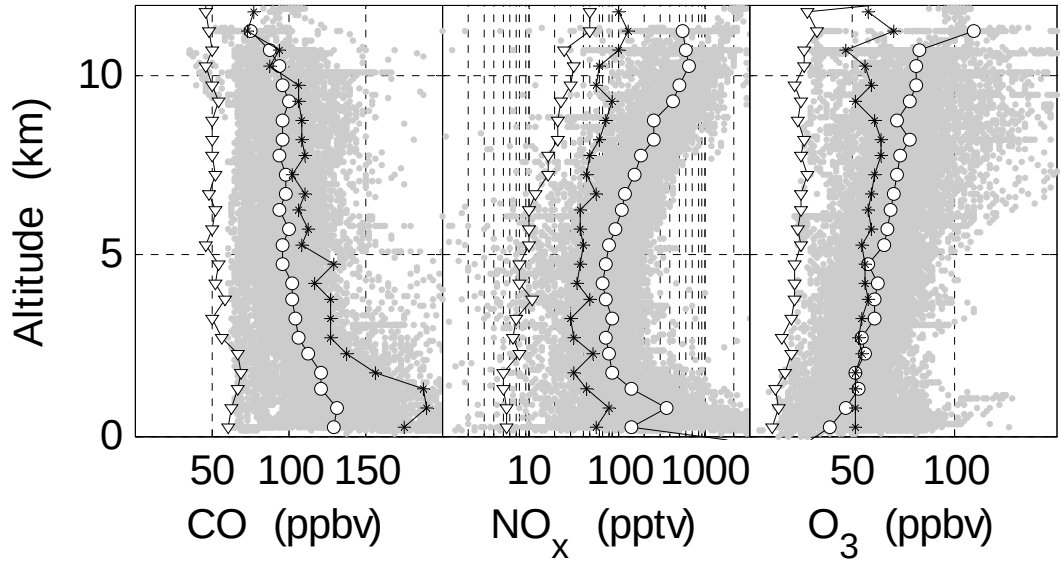

Figure 7. Comparison of NO dependence for (a) OH and (b) HO_2 of (up) measured (circles) and modeled (stars) values and (down) measured-to-modeled ratios in INTEX-A (circles), TRACE-P (stars) and PEM Tropics B (triangles). Individual INTEX-A 1-minute measurements are shown (gray dots). Concentrations of NO calculated in the model are used in this figure.

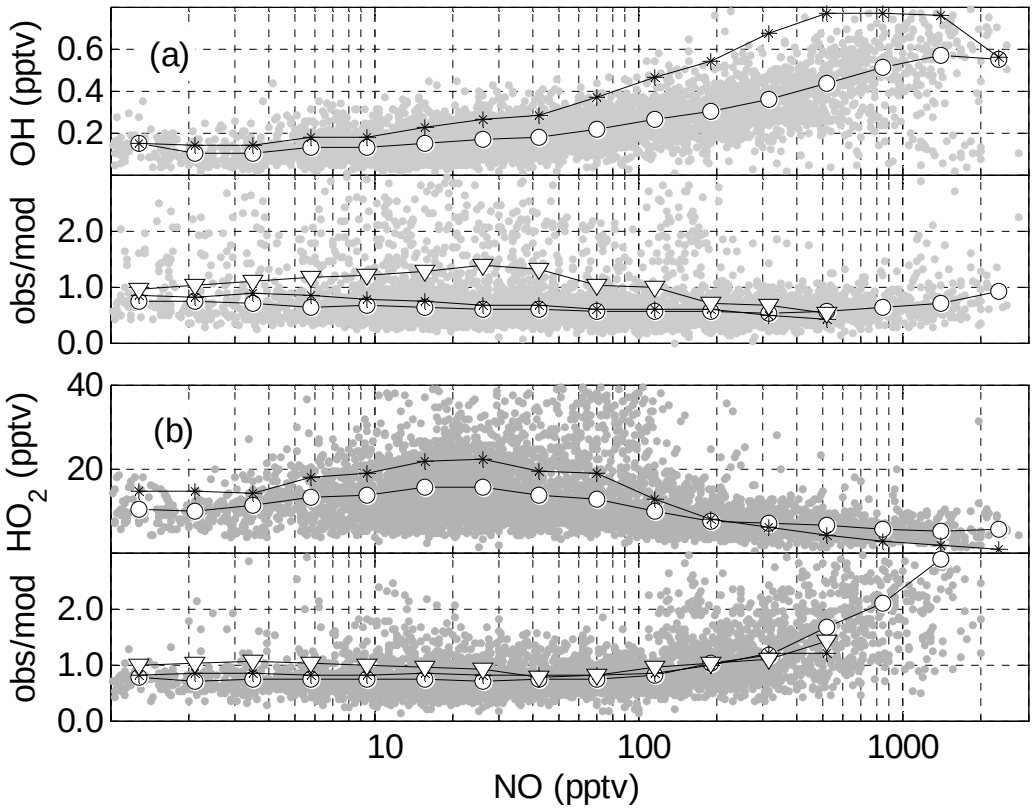

Figure 8. Vertical median profiles of (a) HO_x production: total (thick line), from $O(^1D)+H_2O$ (circles), from HCHO photolysis (stars), and from H_2O_2 photolysis (triangles); and (b) HO_x loss rates: total (thick line), due to HO_2+HO_2/RO_2 (circles), due to $OH+HO_2$ (stars), and due to $OH+NO_x$ (triangles) during INTEX-A. Small gray dots show the 1-minute data for (a) total HO_x production rate and (b) total HO_x loss rate. All the production and loss rates were calculated from the measurements, except for RO_2+HO_2 where RO_2 levels were calculated in the model.

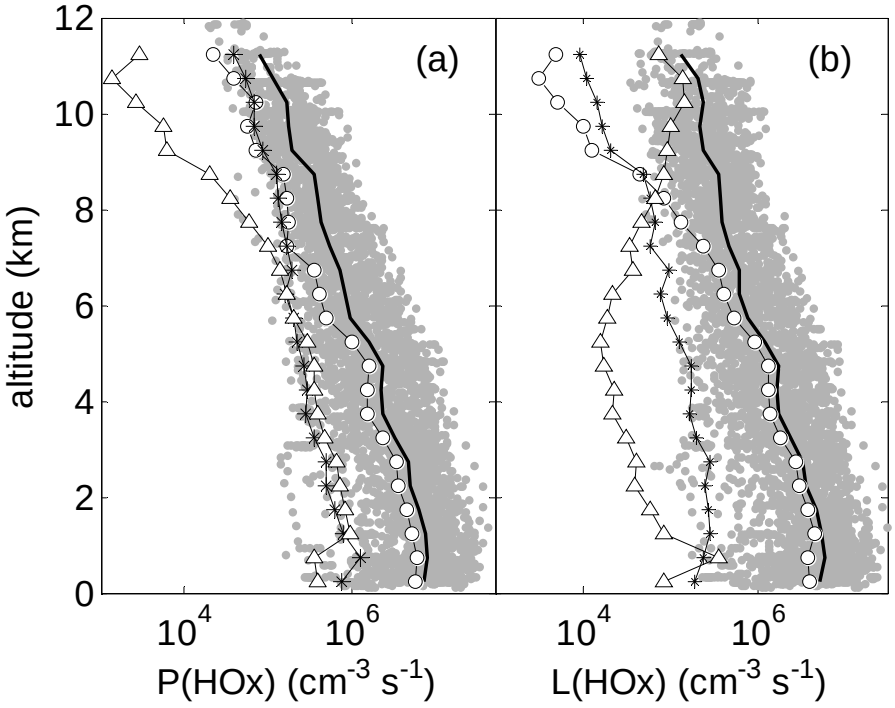

Figure 9. Vertical median profiles of (a) O_3 production rate: total (circles), from HO_2+NO (stars), and from RO_2+NO (triangles) where RO_2 levels were calculated in the model; (b) O_3 loss rate: total (circles), due to $O(^1D)+H_2O$ (stars), due to O_3+OH (triangles), and due to O_3+HO_2 (solid line); and (c) net O_3 production rate during INTEX-A. Small gray dots show the 1-minute data for (a) total O_3 production rate, (b) total O_3 loss rate, and (c) net O_3 production.

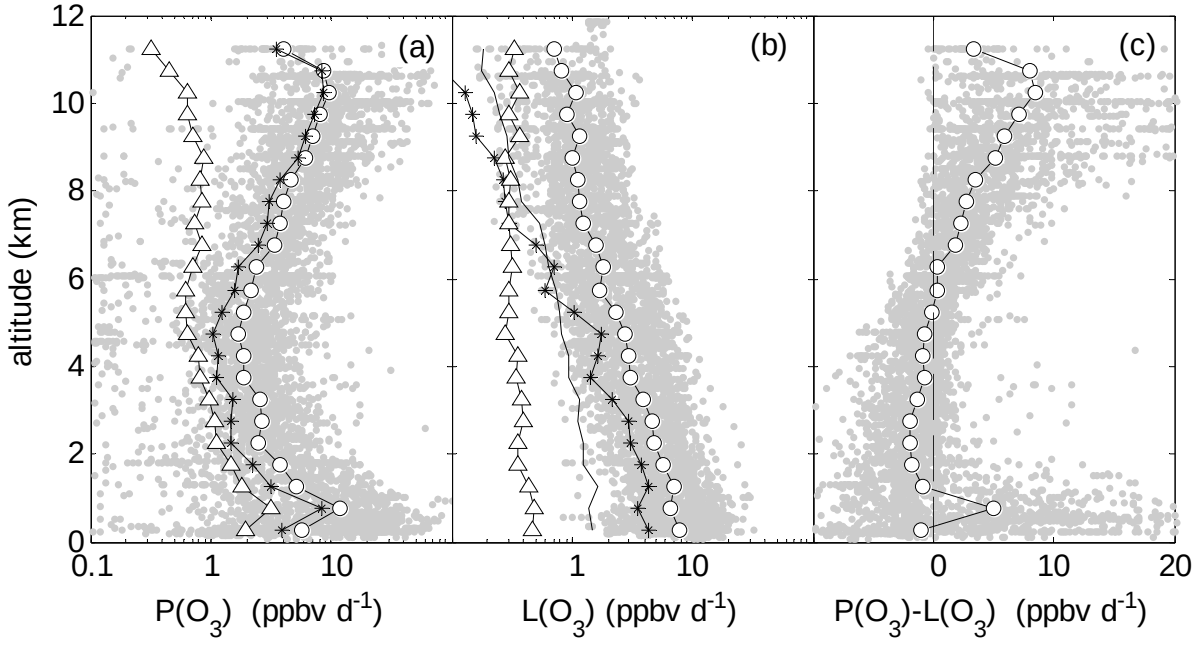

Figure 10. Variation of median H_2O_2 with altitude for the unconstrained instantaneous model (dotted line), the steady-state calculation using observed OH and HO_2 (solid line), and the measurements of the University of Rhode Island (circles) and California Institute of Technology (stars). Steady-state H_2O_2 calculated from observed OH and HO_2 are shown for each minute (gray dots).

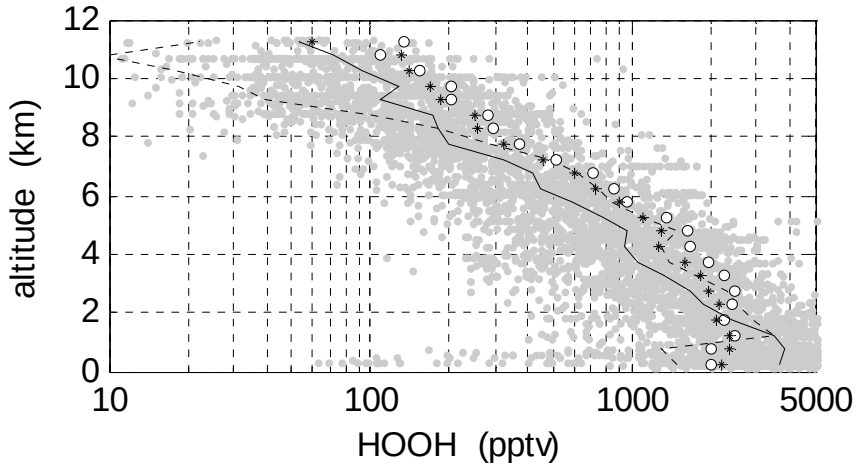

Figure 11. Altitude variation of the calculated OH reactivity (grey dots), altitude-averaged calculated OH reactivity (stars), and the additional OH reactivity needed in the model to bring the measured and modeled HO_2 into agreement (circles).

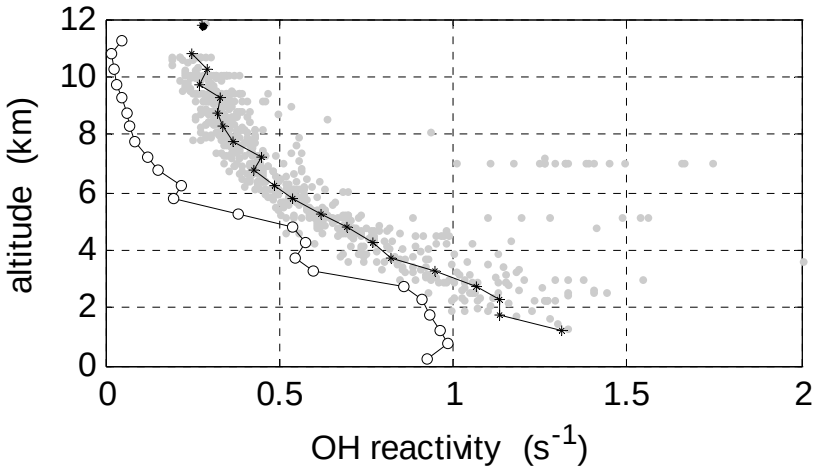

Figure 12. Observed-to-modeled OH, HO_2, and HO_2/OH ratios in stratosphere-influenced air. Shown are 1-km median values (circles and lines) and individual 1-minute values (gray dots).

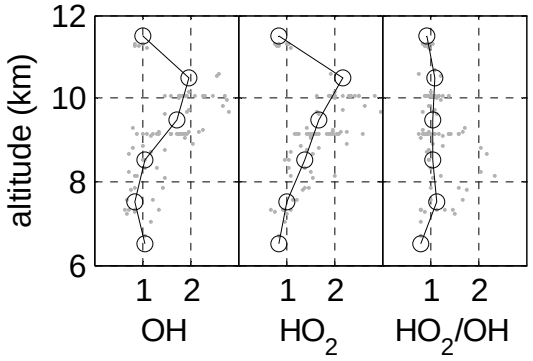

Figure 13. Ratio of constrained-to-unconstrained models for OH (a) and HO_2 (b) as a function of NO. Individual 1-minute comparisons are presented (gray dots) as well as median values (circles and lines).

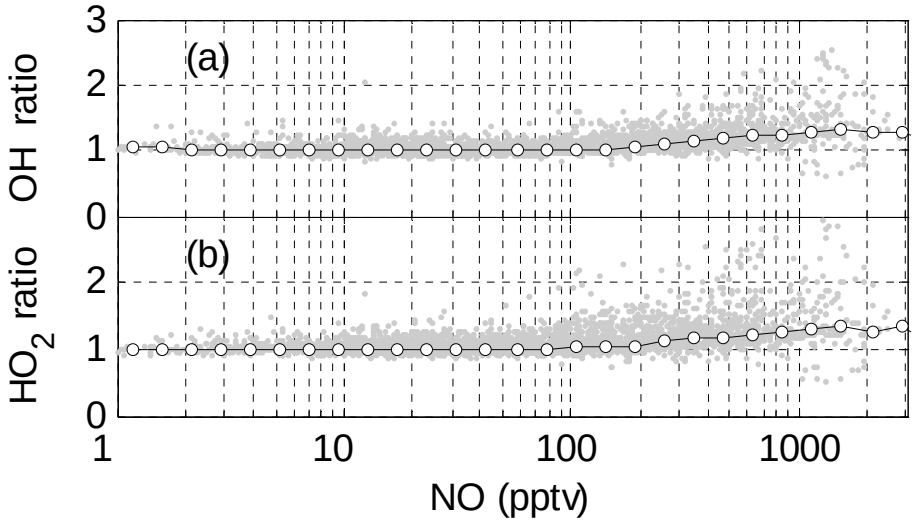

Figure 14. The observed-to-modeled OH ratio as a function of isoprene. Individual 1-minute measurements (gray points) and median values for isoprene intervals (circles) are shown for data taken at less than 1 km altitude and solar zenith angle less than 60^{o}. Median observed-to-modeled OH ratios from the PROPHET tower in a Michigan forest in summer 2000 are also shown (triangles).